Supplementary Information

I. THEORETICAL ESTIMATE

In this section, we show that a $\chi^{(3)}$-based spectral translation process can be comparable to a $\chi^{(2)}$ process through proper nanophotonic mode engineering. We compare the translation efficiency of sum frequency generation (SFG) and degenerate four-wave mixing (dFWM) processes, the results of which were summarized in Fig. 1(d) in the main text. The nonlinear polarization ($\mathcal{P}$) of these two processes at the visible frequency (ω_v) are given by[1]:

$$\mathcal{P}^{(2)}(\omega_v) = 2\varepsilon_0\chi^{(2)}E(\omega_p)E(\omega_t), \tag{S1}$$

$$\mathcal{P}^{(3)}(\omega_v) = 3\varepsilon_0\chi^{(3)}E^2(\omega_p)E^*(\omega_t). \tag{S2}$$

Here ε_0 is the permittivity of free space, $E(\omega_i)$ is the electric field at frequency ω_i, and $i = v, p, t$ represents visible, pump, and telecom wavelengths, respectively. First, we compare these two processes in the waveguide. The light intensity in the waveguide can be estimated as $E(\omega_{p,t}) = \sqrt{2I(\omega_{p,t})/(\varepsilon c)}$ and $\mathcal{P}(\omega_v) = \sqrt{2I(\omega_v)/(\varepsilon c)}$. We assume the material permittivity ε to be the same at all three wavelengths (accurate to first-order) and c is the speed of light in vacuum. The intensity is given by $I = P/A$, where P and A represent optical power and effective mode area, respectively. We assume these two processes take place for the same set of visible/telecom modes and an ideal mode overlap. The ratio of the visible intensities for the two processes in a waveguide, as shown in the black line in Fig. 1(d), is thus given by:

$$Ratio = \left|\frac{\mathcal{P}^{(3)}(\omega_v)}{\mathcal{P}^{(2)}(\omega_v)}\right|^2 = \frac{9}{2}\left|\frac{\chi^{(3)}}{\chi^{(2)}}\right|^2 \frac{P_p}{\varepsilon c A_p}. \tag{S3}$$

In this equation, ε is the permittivity of the $\chi^{(3)}$ medium, and P_p and A_p represent the optical pump power in the waveguide and the effective mode area at the pump wavelength.

The microring parameters we use for comparison are based on the typical geometry in this work (see Table I in the main text for details), and the waveguide shares the same dimensions as the microring cross-section. The wavelengths of interest are 1560 nm and 780 nm for the input signal and translated signal, respectively. Nonlinear refractive indices used in the comparison are $\chi^{(3)} = 3.39\times10^{-21}$ m^2/V^2 ($n_2 = 2.4\times10^{-15}$cm^2/W) and $\chi^{(2)} = 60$ pm/V, which are typical values for Si_3N_4 (Ref. 2) and $LiNbO_3$ (Ref. 1), respectively. We note that many $LiNbO_3$ photonic works quote smaller $\chi^{(2)}$ values due to technical issues (thin film quality, quasi-phase-matching, etc.), but we use the largest bulk nonlinearities for $LiNbO_3$ to give a conservative comparison. The effective area for the pump mode is 0.18 μm^2, simulated by the finite-element method. While the modal confinement provided by a waveguide provides an enhancement over bulk material, the pump power required for a $\chi^{(3)}$ process to be comparable to $\chi^{(2)}$ process is unreasonably large (black line in Fig. 1(d)), and is off the x-axis range displayed.

A high-Q microring provides strong confinement of light in both space and time, resulting in greatly enhanced optical intensities. The enhancement of the optical intensity in the microring can be estimated by its finesse ($\mathcal{F} = Q\frac{FSR}{\omega/2\pi}$). The efficiency ratio $\eta[\chi^{(3)}]/\eta[\chi^{(2)}]$ is thus multiplied by $\mathcal{F}$, as shown by the blue line in Fig. 1. The assumed finesse ($\mathcal{F}$) of the microring is 5000, which corresponds to an optical quality factor of $Q = 10^6$ for a free spectral range (FSR) of 1 THz, consistent with measurements for our device. With the cavity enhancement, the efficiency ratio $\eta[\chi^{(3)}]/\eta[\chi^{(2)}]$ is much larger than it is in a waveguide, but is still only -44 dB at 1 mW. However, for the estimates considered so far, we have assumed perfect mode overlap among the interacting modes, whereas in practice the the mode overlap of the $\chi^{(2)}$ process has usually been less than ideal, while in our $\chi^{(3)}$ device the overlap is close to unity. Taking this factor into account, we have a further enhancement of the efficiency ratio, as shown by the red line in Fig. 1(d). The mode overlap of the $\chi^{(2)}$ process is estimated to be 0.3, which is typical because different and higher-order mode families are used for $\chi^{(2)}$ dispersion matching[3]. An extra factor of 0.043 takes into account the difficulties to identify/employ the targeted modes, which has especially been a problem for mm-scale devices in which many mode families are supported[4]. We note that this extra factor could ideally be removed if optical modes of the same family can be unambiguously identified and frequency-matched and phase-matched in a nanophotonic $\chi^{(2)}$ process. However, this has not been achieved in the context of wide-band nanophotonic spectral translation, to the best of our knowledge.

Although we take SFG and dFWM as examples here, the comparison is generally applicable to $\chi^{(2)}$ and $\chi^{(3)}$ processes. For SHG and non-degenerate FWM, Eq. S1 and Eq. S2 are corrected by a factor of 1/2 and 2, respectively, due to the degenerate/non-degenerate nature of the processes. The estimate of efficiency ratio is therefore within a factor of 4 depending on the exact processes being compared, which does not affect the general trends shown in Fig. 1.

II. EXPERIMENTAL SETUP

The device is tested with the experimental setup shown in Figure S1, which illustrates the measurement configurations for cavity transmission, photon pair spectrum of spontaneous degenerate four-wave mixing (Sp-dFWM), and spectral translation by stimulated degenerate four-wave mixing (St-dFWM). For the cavity transmission measurement, three tunable continuous-wave lasers are used in turn to measure the transmission spectra of the signal, pump, and idler bands. The wavelengths of the cavity modes are calibrated by a wavemeter with an accuracy of 0.1 pm. The pump laser is attenuated to sub-milliwatt levels to avoid thermal bistability with the polarization adjusted to transverse-electric (TE). Pump, visible, and telecom signals are coupled on and off the chip by lensed optical fibers with a focused spot size diameter of $\approx 2.5\ \mu$m. To achieve mode profiles that best match to these fibers, the input/output waveguides are tapered to expand their optical modes, with an oxide lift-off process to make the modes symmetric in the vertical direction. The measured fiber-chip insertion losses are (3.33 ± 0.24) dB, (2.92 ± 0.15) dB, and (2.97 ± 0.09) dB per facet at 669.8 nm, 939.5 nm, and 1572.7 nm, respectively. The uncertainty is calculated as a one standard deviation value from the transmission background (Fig. 3(a) in the main text). These insertion losses are used to calibrate the on-chip pump/telecom power from the measured power in the fiber that is incident on the chip. In measurements of the device's spectrum, no filters are required before the device, since both the laser's amplified-spontaneous-emission noise and the Raman noise generated in the optical fibers have a frequency spectrum that is far from the visible band. When measuring the spectrum of Sp-dFWM and calibrating power-dependent St-dFWM measurements, a free-space dichroic setup is used. The dichroic setup contains fiber-to-free-space coupling, a 950 nm dichroic mirror, two cascaded bandpass filters at 670 nm with 10 nm full-width at half-maximum (FWHM) (providing >80 dB isolation), and free-space-to-fiber coupling for detection. The overall loss for the 670 nm path of the dichroic filter is (3.44 ± 0.06) dB. Since this wavelength is not reachable by our red laser, the loss is calibrated with the optical spectrum analyzer (OSA) by using the spectrally translated signal before/after the dichroic filter. The uncertainty represents one-standard deviation from six measurements, which is likely due to uncertainty from fiber connection and/or OSA detection.

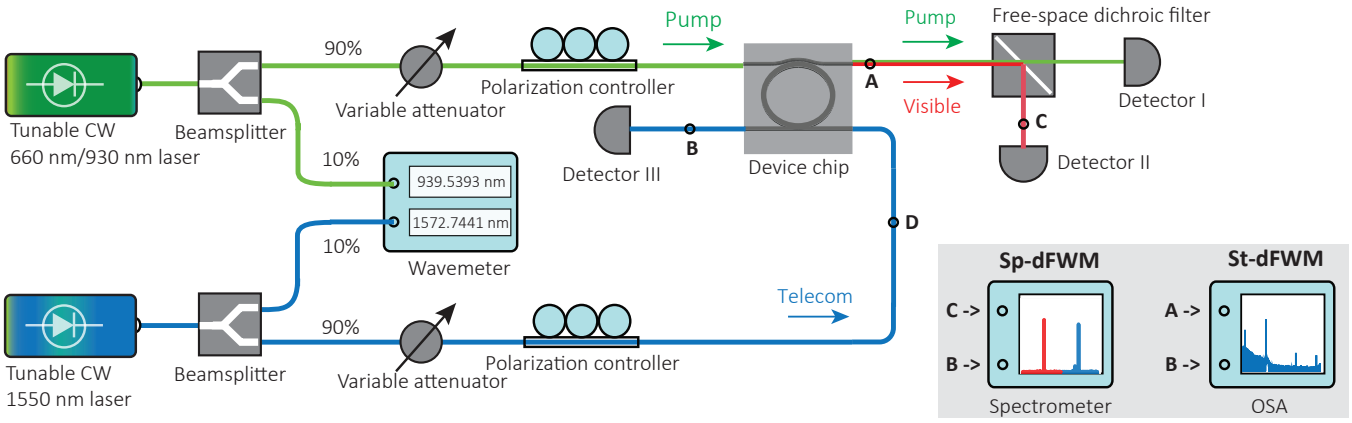

FIG. S1: **Experimental Setup**. Figure of the experimental setup used to record cavity transmission, photon pair spectra by Sp-dFWM, and spectral translation by St-dFWM. CW: continuous-wave. In the Sp-dFWM case, only the 930 nm (pump) laser is used. In the St-dFWM case, 930 nm (pump) and 1550 nm (telecom) lasers are used. Points A-D are used to guide the different configurations in the experiments. Sp-dFWM: spontaneous degenerate four-wave mixing. St-dFWM: stimulated degenerate four-wave mixing.

* Electronic address: xiyuan.lu@nist.gov
† Electronic address: kartik.srinivasan@nist.gov

[1] R. W. Boyd, *Nonlinear Optics* (Academic Press, Amsterdam, 2008).
[2] K. Ikeda, R. E. Saperstein, N. Alic, and Y. Fainman, "Thermal and Kerr nonlinear properties of plasma-deposited silicon nitride/ silicon dioxide waveguides," Opt. Express **16**, 12987–12994 (2008).
[3] V. S. Ilchenko, A. A. Savchenkov, A. B. Matsko, and L. Maleki, "Nonlinear optics and crystalline whispering gallery mode cavities," Physical Review Letters **92**, 043903 (2004).
[4] J. U. Fürst, D. V. Strekalov, D. Elser, M. Lassen, U. L. Andersen, C. Marquardt, and G. Leuchs, "Naturally phase-matched second-harmonic generation in a whispering-gallery-mode resonator," Physical Review Letters **104**, 153901 (2010).